

This is a repository copy of *A fast multiple mode intermediate level circuit model for the prediction of shielding effectiveness of a rectangular box containing a rectangular aperture.*

White Rose Research Online URL for this paper:
<https://eprints.whiterose.ac.uk/132800/>

Article:

Konefal, T, Dawson, J F orcid.org/0000-0003-4537-9977, Marvin, A C orcid.org/0000-0003-2590-5335 et al. (2 more authors) (2005) A fast multiple mode intermediate level circuit model for the prediction of shielding effectiveness of a rectangular box containing a rectangular aperture. IEEE Transactions on Electromagnetic Compatibility. pp. 678-691. ISSN 0018-9375

<https://doi.org/10.1109/TEM.2005.853715>

Reuse

["licenses_typename_other" not defined]

Takedown

If you consider content in White Rose Research Online to be in breach of UK law, please notify us by emailing eprints@whiterose.ac.uk including the URL of the record and the reason for the withdrawal request.

A fast multiple mode intermediate level circuit model for the prediction of shielding effectiveness of a rectangular box containing a rectangular aperture

T. Konefal, J.F. Dawson, A.C. Marvin, M. P. Robinson and S.J. Porter

Abstract

This paper presents an intermediate level circuit model (ILCM) for the prediction of the shielding effectiveness (SE) of a rectangular box containing a rectangular aperture, irradiated by a plane wave. The ILCM takes into account multiple waveguide modes, and is thus suitable for use at high frequencies and/or relatively large boxes. Inter-mode coupling and reradiation from the aperture are taken into account. The aperture may be positioned anywhere in the front face of the box, and the SE at any point within the box may be found. The model is presented in such a way that existing ILCM techniques for modelling elements such as monopoles, dipoles, loops or transmission lines may be seamlessly incorporated into the circuit model. Solution times using the ILCM technique are hundreds of times less than those required by traditional numerical methods such as FDTD, TLM or MoM, even when using a relatively slow interpreted language such as MATLAB. Accuracy however is not significantly compromised. Comparing the circuit model with TLM over nine data sets from 4MHz to 3GHz resulted in an rms difference of 7.70dB and mean absolute difference of 5.55dB in the predicted SE values.

Keywords: Circuit model, multiple modes, shielding effectiveness, aperture in box.

1 Introduction

A frequently occurring problem in electromagnetic compatibility (EMC) is the determination of the electromagnetic fields inside an enclosure containing apertures. In many cases the enclosure and apertures are rectangular, and this has led to a number of attempts at solving the problem of a rectangular box with a rectangular aperture, irradiated by a plane wave. For example, in [1-4] the electric field integral equation (EFIE) is used to solve the problem using the Method of Moments (MoM). Although the treatment of the aperture is efficient, this self-consistent method is still computationally intensive. Indeed, using a variety of standard numerical techniques such as Finite Difference Time Domain (FDTD), Transmission Line Matrix (TLM) or Method of Moments (MoM), the problem is readily tackled e.g. [5-7]. Unfortunately there can often be some differences in the solutions in critical regions using these techniques, depending on the slight differences in spatial, time or frequency resolution chosen for the computer simulations, and indeed on the precise simulation method chosen. A purely analytic approach is described in [6], though even in this case we are forced to truncate an infinite series at some suitable point, and the method effectively becomes a MoM solution. However, the main problem with such techniques is that they all require significant computer resources such as RAM and/or hard disk space, and can take several hours, days or even weeks to reach a solution. This is true despite the

significant and continuing improvement that has been made in commonly available computing resources in recent years. (Clock speeds of 2-3GHz are typical of computing equipment at the time of writing).

The slowness of solution using these methods has prompted a number of investigators to try and find a more rapid solution to the problem, using various approximations. One of the first successful techniques was that due to Robinson et al. [8], who used an equivalent circuit technique to find a sufficiently accurate frequency domain solution to the problem in just a few lines of computer code, taking only a small fraction of a second. The original solution of [8] is limited in its scope in a number of ways. The incident plane wave can only have one polarization and direction of travel, though fortunately this is often the worst case as far as shielding effectiveness (SE) is concerned. In addition, the rectangular slot must be centrally placed in both height and width in the rectangular front face of the box. However, the most severe limitation of the model in [8] is that the model considers only the excitation of the TE_{10} mode of the box. This limits the accuracy of the solution to low frequencies and/or relatively small boxes, where the TE_{10} mode is dominant. We note here that the model has no difficulty with dealing with an exponentially decaying (evanescent) mode, below the TE_{10} cut off frequency. However, at frequencies where higher order modes can propagate, the model becomes inaccurate. For reasonably large boxes, of the order $0.1m^3$, the scope of the model in [8] is thus limited to a few hundred MHz.

The problem of oblique incidence of irradiation has been addressed in [9], whilst still retaining only the TE_{10} mode. The aperture is treated as a two-wire transmission line with no radiation losses. The treatment is extended in [10] to take into account multiple modes, though only frequencies below 1GHz are considered. In fact, only one of the results presented in [10] involves a higher order propagating mode below 1GHz, and in this particular case there is a feature in the predicted SE just below 700MHz, corresponding to the TE_{201} resonance [11], which is not observed in experiment. (In this particular case the TE_{20} mode begins to propagate above 621MHz). Another attempt at a multimode treatment of the aperture in a box problem has been made in [12], though curiously only TE_{m0} and TM_{1n} modes are considered, making the theory totally unsuitable for prediction of SE for off-centre positions in the box. Indeed, no direct comparisons with numerical results on the same graph are given, and an unknown empirical loss factor is introduced into the model. In all of the models [8-10] and [12], only apertures centrally placed in height and width in the front face of the box are considered.

In this paper we present a multimode intermediate level circuit model (ILCM) for the problem of a rectangular aperture in a rectangular box. The circuit model is presented in such a way that existing ILCM techniques [13-15] may be used to further model the presence of such elements as monopoles, dipoles, loops or microstrip transmission lines inside the box, though for simplicity we limit ourselves in this paper to an empty box. The technique of multimode analogous transmission line circuit theory [16][14] is used to model the modal excitation and coupling of modes in the aperture. In addition, a simple and rapid use of the Numerical Electromagnetics Code (NEC) [17] is made to estimate the radiation resistance of a simple dipole over the frequency range considered. The radiation resistance is converted via Babinet's principle [18] to an equivalent radiation resistance at the centre of the aperture in the front face of the box. Using a method similar to that in [9], the electric field in the aperture is calculated, but in the presence

of the radiation resistance. The resultant aperture field is used to give a first estimate of the modal excitation of the box, under the temporary assumption that the presence of the box does not affect the aperture field. However, unlike the model of [10], the aperture field is then allowed to be altered by energy entering and exiting the box, taking into account inter-mode coupling and energy reradiation into free space. The model thus accounts for all the physical processes present.

The ILCM model can cope with rectangular apertures positioned anywhere in the front face of the box, unlike the models of [8-10] and [12]. However, it is most accurate for ‘slot’ type apertures where the height of the slot is significantly less than its length (say less than 12%). Any direction of incidence and polarisation of the incoming plane wave may be dealt with in the theory, though we have only been concerned with \hat{y} polarized waves travelling in the $+\hat{z}$ direction. In addition, the model can readily be used at high frequencies (we have set an upper limit of 3GHz for convenience) without deterioration in accuracy, providing an appropriate number of modes are taken into account.

The circuit model is rapid, taking typically less than 30 seconds to process 750 frequency data points using a relatively slow interpreted language such as MATLAB. This contrasts with a typical run time of four and a half hours for the numerical technique of Transmission Line Matrix (TLM) modelling. Despite its simplicity, the ILCM model is remarkably accurate, showing an overall rms difference in SE values of 7.70dB compared with TLM, and a mean absolute difference of 5.55dB. Visual examination of the curves in Section 6 supports the validity of the circuit model, with the vast majority of the many features in the TLM simulations reproduced by the circuit theory.

Sections 2 and 3 describe the problem at hand, and give an initial solution for the field in the aperture, in the absence of the rest of the box. Sections 4 and 5 explain how this aperture field is modified by the presence of the box, and develop an equivalent circuit to model the inter-mode coupling and reradiation into free space. The circuit model results are compared with the numerical method of TLM in Section 6, with some conclusions being drawn in Section 7.

2 Plane wave excitation of a rectangular box containing a rectangular slot

2.1 Experimental Configuration

Figure 1 shows the experimental configuration that it is desired to model using circuit theory. A rectangular box of dimensions $a(x) \times b(y) \times d(z)$ contains a rectangular aperture in its front face ($z = 0$) extending from $x = x_l$ to $x = x_h$ and $y = y_l$ to $y = y_h$. The box is irradiated by an incident plane wave E_y^{inc} , polarized in the \hat{y} direction and travelling in the $+\hat{z}$ direction. The aperture is assumed to be ‘slot’ like, so that $(y_h - y_l) < (x_h - x_l)$, but otherwise may be positioned anywhere on the front panel. In addition, the slot height $(y_h - y_l)$ is considered to be

much less than a wavelength of free space radiation at the frequency of irradiation of E_y^{inc} . Under these conditions, and particularly if $(y_h - y_l) \ll (x_h - x_l)$, the slot can be approximated to a section of coplanar strip transmission line that has been short-circuited at x_l and x_h . When the aperture or slot is centrally placed in the front panel, it is possible to assign a quasi-static characteristic impedance to this transmission line [19]. However, for the purposes of this paper we need the slot transmission line to have the same characteristic impedance as the quasi-TEM wave it supports. This is necessary to be consistent with the general theory of analogous transmission lines described in [14][20], where the analogous transmission line representing a waveguide mode is assigned the same characteristic impedance as the transverse ratio of E and H fields that the mode supports. The ‘analogous’ transmission line (rather than the literal transmission line) representing the slot is therefore assigned a characteristic impedance of $Z_{FS} = 377\Omega$, the impedance of free space. This assignment is not only found to improve the quality of the results (see Section 6) but also negates the need to work out the characteristic impedance when the slot is not placed at the central height of the front panel.

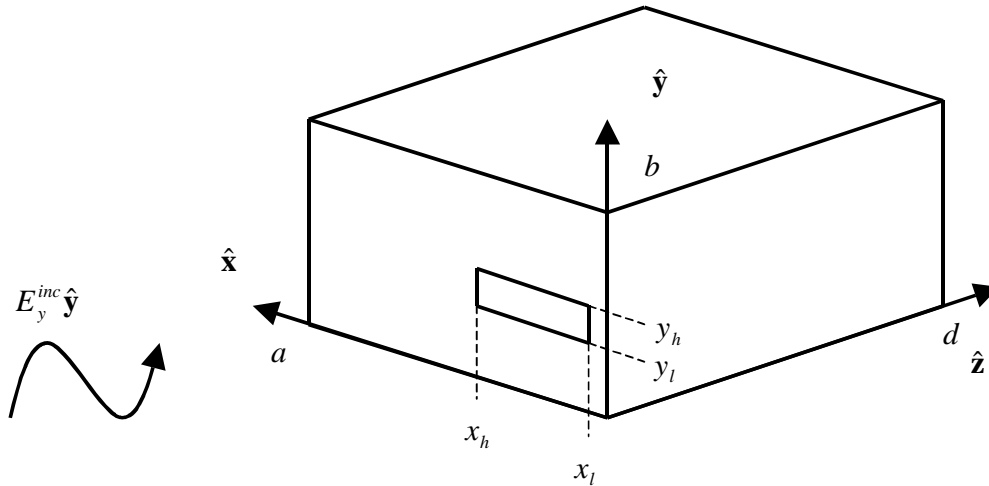


Figure 1. Slot in box irradiated by incident field E_y^{inc} , showing box dimensions and slot dimensions.

2.2 Plane wave excitation of a two-wire transmission line

The analysis in this section is similar to that given in [9]. Consider a two-wire transmission line of length $x_h - x_l$ aligned in the \hat{x} direction and with a vertical separation $g = y_h - y_l$ in the \hat{y} direction. The line is situated in the plane $z = 0$ and is illuminated by a plane wave travelling in the direction $\hat{\mathbf{b}}$. The incident electric and magnetic fields are related by

$$Z_{FS} \mathbf{H}^{inc} = \hat{\mathbf{b}} \times \mathbf{E}^{inc} \quad (1)$$

where

$$\mathbf{E}^{inc} = (E_x^{inc}, E_y^{inc}, E_z^{inc}) \exp(-j\boldsymbol{\beta} \cdot \mathbf{r}) \quad (2)$$

$$\mathbf{H}^{inc} = (H_x^{inc}, H_y^{inc}, H_z^{inc}) \exp(-j\boldsymbol{\beta} \cdot \mathbf{r}) \quad (3)$$

$$\boldsymbol{\beta} = (\beta_x, \beta_y, \beta_z) = |\boldsymbol{\beta}| \hat{\mathbf{b}} = \frac{\omega}{c} \hat{\mathbf{b}} \quad (4)$$

The transmission line equations of the system, including the forcing terms of the external applied fields, can be solved as in [9] to give the voltage $V(x)$ on the transmission line i.e.

$$V(x) = A \exp\left(+j\frac{\omega}{c}x\right) + B \exp\left(-j\frac{\omega}{c}x\right) + H \exp(-j\beta_x x) \quad (5)$$

where

$$H = \frac{\left[\frac{\omega^2}{c^2} E_y^{inc} + \omega \mu_0 \beta_x H_z^{inc} \right] T_y}{\frac{\omega^2}{c^2} - \beta_x^2} \quad (\beta_x \neq \frac{\omega}{c}) \quad (6)$$

$$T_y = \begin{cases} \left[\frac{\exp(-j\beta_y y)}{-j\beta_y} \right]_{y_l}^{y_h} & \text{for } \beta_y \neq 0 \\ y_h - y_l & \text{for } \beta_y = 0 \end{cases} \quad (7)$$

and A and B are determined by the boundary conditions of short circuits terminating the line in the planes $x = x_l$ and $x = x_h$ i.e. $V(x_l) = V(x_h) = 0$. Thus

$$\begin{bmatrix} A \\ B \end{bmatrix} = \begin{bmatrix} \exp(+j\omega x_h / c) & \exp(-j\omega x_h / c) \\ \exp(+j\omega x_l / c) & \exp(-j\omega x_l / c) \end{bmatrix}^{-1} \begin{bmatrix} -H \exp(-j\beta_x x_h) \\ -H \exp(-j\beta_x x_l) \end{bmatrix} \quad (8)$$

Equations 5-8 define the solution to the voltage $V(x)$ on the two-wire transmission line.

The solution of Equation 5 can be used to find the field E_y^{wire} between the two wires of the transmission line i.e.

$$E_y^{wire} = -\frac{V(x)}{y_h - y_l} = -\frac{V(x)}{g} = -\frac{A}{g} \exp\left(+j\frac{\omega}{c}x\right) - \frac{B}{g} \exp\left(-j\frac{\omega}{c}x\right) - \frac{H}{g} \exp(-j\beta_x x) \quad (9)$$

We now make the assumption that the field $E_y^{aperture}(x)$ in the slot of Figure 1, in the absence of the rest of the box in the region $z > 0$, is approximately a factor (b/g) times larger than E_y^{wire} , to account for the extended width of the transmission line conductors, occupying the regions

$0 \leq y \leq y_l$ and $y_h \leq y \leq b$. Providing b is small compared to a wavelength, this should be a good assumption, since when viewed in the plane $z = 0$ the two-wire transmission line appears as a short dipole whose length has been extended by the factor (b/g) , with a corresponding increase in antenna factor of (b/g) . This should also serve as a reasonable first approximation for the increase in field when b is comparable to a wavelength. The aperture field in Figure 1, in the absence of the rest of the box in the region $z > 0$, is thus estimated as

$$E_y^{aperture}(x) = -\frac{b}{g^2} \left[A \exp\left(+j\frac{\omega}{c}x\right) + B \exp\left(-j\frac{\omega}{c}x\right) + H \exp(-j\beta_x x) \right] \quad (10)$$

Equation 10 does not take into account the energy that enters and exits the box, nor does it take into account (in free space) any reradiated energy. The latter aspect is dealt with in the next section, which uses the Numerical Electromagnetics Code (NEC) [17] in conjunction with the Babinet principle [18] to assign a radiation resistance to the original two-wire transmission line problem. This modifies the solution for $E_y^{aperture}(x)$ given by Equation 10 and significantly reduces the Q factor of the undesirable strong resonance that would otherwise occur when the slot length $(x_h - x_l)$ corresponds to a half wavelength of radiation. Note that Equation 10 permits arbitrary angles of incidence for a plane wave, though for the sake of brevity we have been concerned in this paper only with plane waves for which $\beta_x = 0, \beta_y = 0$.

3 Modification of the aperture field in free space by inclusion of radiation resistance

3.1 Use of NEC to find radiation resistance

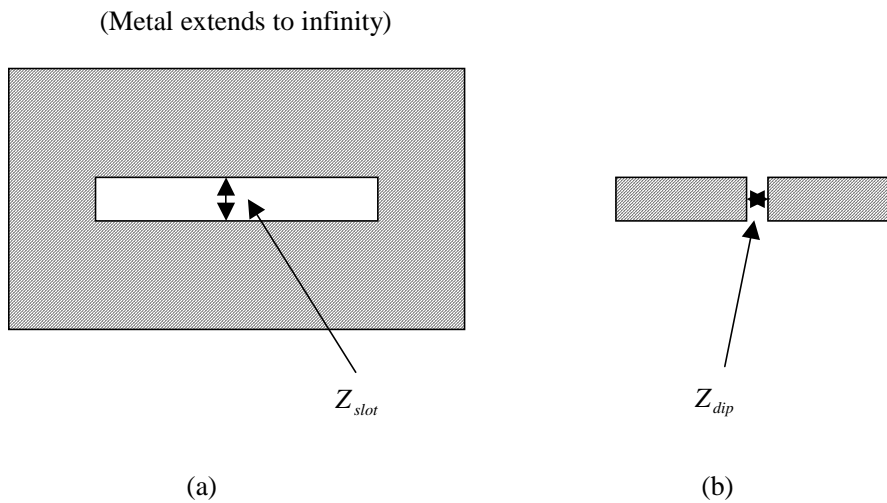


Figure 2. Complementary structures illustrating the Babinet principle.

Figure 2 shows two complementary structures where metal is replaced by free space and vice versa. From Babinet's principle [18] the impedances of the two structures at the points shown are related by

$$Z_{slot} Z_{dip} = \frac{Z_{FS}^2}{4} \quad (11)$$

where Z_{FS} is the impedance of free space ($Z_{FS} = 377\Omega$). In order to find the impedance Z_{slot} therefore, we simulate the impedance of the planar dipole of Figure 2(b) using the Numerical Electromagnetics Code (NEC) [17]. This is very rapid, and typically will take less than a second for 750 data points. In practice, if the width w and the length l of the planar strip are $w = y_h - y_l$, $l = x_h - x_l$, a reasonable approximation to the impedance Z_{dip} can be found by simulating the impedance at the centre of a wire dipole of length l and radius r where $\pi r = w$. From Equation 11, the corresponding impedance Z_{slot} of Figure 2(a) may be found. Note that the NEC simulation will generate a value of Z_{dip} which has a real component, representing the radiation loss mechanism into free space. Similarly, Z_{slot} will have a real component, also representing the radiation loss mechanism into free space. It is this resistance which is used to modify the solutions for $V(x)$ and $E_y^{aperture}(x)$ given by Equations 5 and 10 respectively, in the absence of reradiation from the slot. Note that we do not in fact have an infinite sheet of metal surrounding our slot in Figure 2, so that this treatment is approximate.

3.2 Calculation of parallel radiation resistance of slot

From simulation using NEC, the impedance of the dipole of Figure 2(b) is given by

$$Z_{dip} = R_d + jX_d \quad (12)$$

From the transmission line point of view, Z_{slot} in Figure 2 can be considered as two short circuited sections of transmission line connected in parallel (a pure reactance) in parallel with a radiation resistance R_p . Manipulating Equations 11 and 12 yields the parallel radiation resistance R_p in terms of the dipole resistance R_d simulated in NEC as

$$R_p = \frac{Z_{FS}^2}{4R_d} \quad (13)$$

Thus from NEC simulation of the dipole in Figure 2(b), it is possible via Equations 12 and 13 to find the equivalent radiation resistance R_p strapped across the centre of the slot in Figure 2(a). The next section explains how to calculate the aperture field $E_y^{aperture}(x)$ in the presence of this radiation resistance.

3.3 Solution for aperture field $E_y^{aperture}(x)$ in the presence of R_p

Figure 3 illustrates a two-wire transmission line, irradiated externally by a plane wave travelling in the $\hat{\mathbf{b}}$ direction. In the absence of any reradiation from the line, the solution for the electric field between the wires is given by the aperture field $E_y^{aperture}(x)$ in Equation 10 with $b = y_h - y_l = g$.

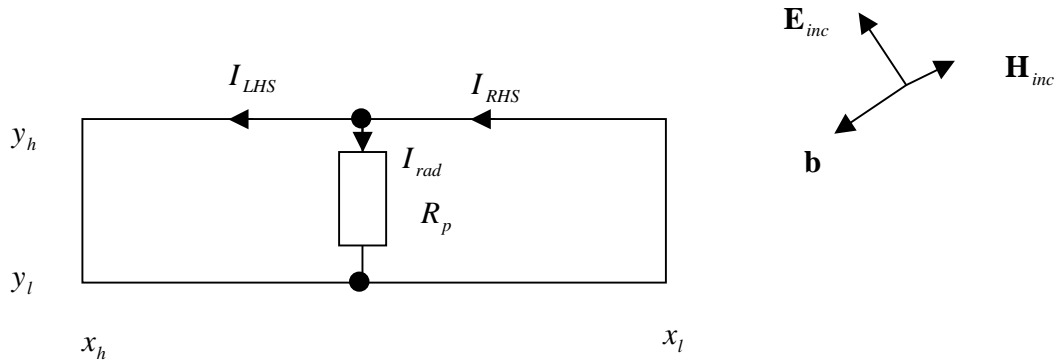


Figure 3. Transmission line with radiation resistance R_p , irradiated by plane wave.

We wish to calculate the field on the line in the presence of R_p , the radiation resistance that enables energy to be lost from the line by the process of reradiation. Following the method in Section 2.2, we can write the solution for the voltages on the left hand side (LHS) and the right hand side (RHS) of R_p as

$$V_{LHS}(x) = A_L \exp\left(+j\frac{\omega}{c}x\right) + B_L \exp\left(-j\frac{\omega}{c}x\right) + H \exp(-j\beta_x x) \quad (14)$$

$$V_{RHS}(x) = A_R \exp\left(+j\frac{\omega}{c}x\right) + B_R \exp\left(-j\frac{\omega}{c}x\right) + H \exp(-j\beta_x x) \quad (15)$$

with corresponding solutions for the LHS and RHS currents given by

$$Z_{0s} I_{LHS}(x) = -A_L \exp\left(+j\frac{\omega}{c}x\right) + B_L \exp\left(-j\frac{\omega}{c}x\right) + Z_{0s} H' \exp(-j\beta_x x) \quad (16)$$

$$Z_{0s} I_{RHS}(x) = -A_R \exp\left(+j\frac{\omega}{c}x\right) + B_R \exp\left(-j\frac{\omega}{c}x\right) + Z_{0s} H' \exp(-j\beta_x x) \quad (17)$$

Here Z_{0s} is the characteristic impedance of the transmission line (which we will eventually take to be $Z_{FS} = 377\Omega$) and

$$H' = \frac{[\omega\beta_x E_y^{inc} + \omega^2 \mu_0 H_z^{inc}] C_l T_y}{\frac{\omega^2}{c^2} - \beta_x^2} \quad (\beta_x \neq \frac{\omega}{c}) \quad (18)$$

Here C_l is the capacitance per unit length of the line. In fact H' is irrelevant in the analysis that follows, so that we do not need to know the value of C_l explicitly. H is given by Equation 6 as before. The coefficients A_L , B_L , A_R and B_R need to be determined by four independent boundary conditions for the circuit in Figure 3. These four boundary conditions are as follows:

$$V_{LHS}(x_h) = 0 \quad (19)$$

$$V_{RHS}(x_l) = 0 \quad (20)$$

$$V_{LHS}(x_m) = V_{RHS}(x_m) \quad (21)$$

$$I_{LHS}(x_m) = I_{RHS}(x_m) - V_{RHS}(x_m)/R_p \quad (22)$$

where the mid point of the line is at $x_m = (x_l + x_h)/2$. Combining these boundary conditions with Equations 14-17 yields the following matrix equation:

$$\begin{bmatrix} \exp\left(+j\frac{\omega}{c}x_h\right) & \exp\left(-j\frac{\omega}{c}x_h\right) & 0 & 0 \\ 0 & 0 & \exp\left(+j\frac{\omega}{c}x_l\right) & \exp\left(-j\frac{\omega}{c}x_l\right) \\ \exp\left(+j\frac{\omega}{c}x_m\right) & \exp\left(-j\frac{\omega}{c}x_m\right) & -\exp\left(+j\frac{\omega}{c}x_m\right) & -\exp\left(-j\frac{\omega}{c}x_m\right) \\ -\exp\left(+j\frac{\omega}{c}x_m\right) & \exp\left(-j\frac{\omega}{c}x_m\right) & \left[\frac{Z_{0s}}{R_p} + 1\right]\exp\left(+j\frac{\omega}{c}x_m\right) & \left[\frac{Z_{0s}}{R_p} - 1\right]\exp\left(-j\frac{\omega}{c}x_m\right) \end{bmatrix} \times \begin{bmatrix} A_L \\ B_L \\ A_R \\ B_R \end{bmatrix} = \begin{bmatrix} -H \exp(-j\beta_x x_h) \\ -H \exp(-j\beta_x x_l) \\ 0 \\ -\frac{Z_{0s}}{R_p} H \exp(-j\beta_x x_m) \end{bmatrix} \quad (23)$$

The coefficients A_L , B_L , A_R and B_R can now be found by a simple matrix inversion, and the solution for the voltage on the two wire line in Figure 3 is defined by Equations 14 and 15. The field $E_y^{aperture}(x)$ in the two-wire line is given by $-V_{L/RHS}(x)/(y_h - y_l)$. As before, this field is multiplied by a factor $b/(y_h - y_l)$ to account for the extended vertical height b of the box in Figure 1. The field in the aperture, in the absence of the rest of the box in the region $z > 0$, is thus given by

$$E_y^{aperture}(x) = -\frac{b}{(y_h - y_l)^2} \left[A_R \exp\left(+j\frac{\omega}{c}x\right) + B_R \exp\left(-j\frac{\omega}{c}x\right) + H \exp(-j\beta_x x) \right] \quad (24)$$

$$\text{for } x_l \leq x \leq x_m$$

and

$$E_y^{aperture}(x) = -\frac{b}{(y_h - y_l)^2} \left[A_L \exp\left(+j\frac{\omega}{c}x\right) + B_L \exp\left(-j\frac{\omega}{c}x\right) + H \exp(-j\beta_x x) \right] \quad (25)$$

$$\text{for } x_m \leq x \leq x_h$$

This aperture field is of course modified by the reaction of energy that enters and exits the rest of the box in the region $z > 0$ in Figure 1. Sections 4 and 5 explain how this is dealt with in terms of modal analogous transmission line theory, and how this leads to the entire field problem being expressed in terms of an equivalent circuit problem.

4 Excitation of modes in infinitely long waveguide by aperture field. Equivalent circuit representation and the principle of reciprocity

4.1 Excitation of modes by aperture field

For an infinitely long waveguide, or alternatively an absorbing wall in the plane $z = d$ in Figure 1, the fields E_y and E_x inside the waveguide can be expressed as a sum of forward travelling TE and TM modes i.e.

$$E_y(\mathbf{r}) = \sum_{m=1}^{\infty} \sum_{n=0}^{\infty} C_{fmn}^{TE} \exp(-\gamma_{mn} z) \left(\frac{m\pi}{a} \right) \sin\left(\frac{m\pi x}{a} \right) \cos\left(\frac{n\pi y}{b} \right) + \sum_{m=1}^{\infty} \sum_{n=1}^{\infty} C_{fmn}^{TM} \exp(-\gamma_{mn} z) \left(\frac{n\pi}{b} \right) \sin\left(\frac{m\pi x}{a} \right) \cos\left(\frac{n\pi y}{b} \right) \quad (26)$$

$$\begin{aligned}
E_x(\mathbf{r}) = & -\sum_{m=0}^{\infty} \sum_{n=1}^{\infty} C_{fmn}^{TE} \exp(-\gamma_{mn} z) \cos\left(\frac{n\pi}{b}\right) \cos\left(\frac{m\pi x}{a}\right) \sin\left(\frac{n\pi y}{b}\right) \\
& + \sum_{m=1}^{\infty} \sum_{n=1}^{\infty} C_{fmn}^{TM} \exp(-\gamma_{mn} z) \cos\left(\frac{m\pi}{a}\right) \cos\left(\frac{m\pi x}{a}\right) \sin\left(\frac{n\pi y}{b}\right)
\end{aligned} \tag{27}$$

where γ_{mn} is given by

$$\gamma_{mn} = \sqrt{\mu_0 \varepsilon_0 (\omega_c^2 - \omega^2)} \tag{28}$$

$$\omega_c^2 \mu_0 \varepsilon_0 = \left(\frac{m\pi}{a}\right)^2 + \left(\frac{n\pi}{b}\right)^2 \tag{29}$$

The individual coefficients C are as yet unknown, but as we shall see below, with some approximations they can ultimately be expressed in terms of the aperture field.

If we evaluate $E_y(\mathbf{r}) = E_y|_{z=0}$ from Equation 26 in the plane $z = 0$, multiply by $\cos\left(\frac{u\pi y}{b}\right)$ where $u = 0, 1, 2, \dots$ and integrate with respect to y from $y = 0$ to $y = b$ we obtain

$$\begin{aligned}
\int_0^b E_y|_{z=0} \cos\left(\frac{u\pi y}{b}\right) dy = & \sum_{m=1}^{\infty} C_{fmu}^{TE} \left(\frac{m\pi}{a}\right) \sin\left(\frac{m\pi x}{a}\right) \frac{b}{2} (1 + \delta_{u0}) \\
& + \sum_{m=1}^{\infty} C_{fmu}^{TM} \left(\frac{u\pi}{b}\right) \sin\left(\frac{m\pi x}{a}\right) \frac{b}{2} (1 + \delta_{u0})
\end{aligned} \tag{30}$$

where δ_{u0} is the Kronecker-delta symbol, equal to unity for $u = 0$ and zero for $u \geq 1$.

We now require $E_y|_{z=0}$ to equal zero for $0 \leq y \leq y_l$ and $y_h \leq y \leq b$ (zero tangential electric field at a metal surface). We further assume that $E_y|_{z=0}$ in the aperture is in fact independent of y . This will be a very good approximation if the slot is narrow, or at least if the width $g = y_h - y_l$ of the slot is small compared to a wavelength of radiation. Under these assumptions, we can evaluate the left hand side of Equation 30 to give

$$E_y^{ap-actual}(x) \int_{y_l}^{y_h} \cos\left(\frac{u\pi y}{b}\right) dy = E_y^{ap-actual}(x) \times N_u \tag{31}$$

where

$$N_u = \begin{cases} y_h - y_l & u = 0 \\ \frac{b}{u\pi} \left\{ \sin\left(\frac{u\pi y_h}{b}\right) - \sin\left(\frac{u\pi y_l}{b}\right) \right\} & u \geq 1 \end{cases} \tag{32}$$

Combining Equations 31 and 30, we obtain

$$N_u E_y^{ap-actual}(x) = \sum_{m=1}^{\infty} \left\{ C_{fmu}^{TE} \left(\frac{m\pi}{a} \right) + C_{fmu}^{TM} \left(\frac{u\pi}{b} \right) \right\} \sin \left(\frac{m\pi x}{a} \right) \frac{b}{2} (1 + \delta_{uo}) \quad (33)$$

Equation 33 holds for each value of u . Hence putting $u = 0$ results in

$$E_y^{ap-actual}(x) = \frac{b}{N_0} \sum_{m=1}^{\infty} C_{fm0}^{TE} \left(\frac{m\pi}{a} \right) \sin \left(\frac{m\pi x}{a} \right) \quad (34)$$

Putting $u = n \geq 1$ into Equation 33 results in

$$E_y^{ap-actual}(x) = \frac{b}{2N_n} \sum_{m=1}^{\infty} \left\{ C_{fmn}^{TE} \left(\frac{m\pi}{a} \right) + C_{fmn}^{TM} \left(\frac{n\pi}{b} \right) \right\} \sin \left(\frac{m\pi x}{a} \right) \quad (35)$$

Clearly the aperture field $E_y^{ap-actual}(x)$ has a unique Fourier series expansion involving only sine functions, so that we can equate the coefficients of $\sin \left(\frac{m\pi x}{a} \right)$ in Equations 34 and 35. Thus, for $m = 1, 2, 3, \dots$ and $n = 1, 2, 3, \dots$

$$\frac{1}{N_0} C_{fm0}^{TE} \left(\frac{m\pi}{a} \right) = \frac{1}{2N_n} \left\{ C_{fmn}^{TE} \left(\frac{m\pi}{a} \right) + C_{fmn}^{TM} \left(\frac{n\pi}{b} \right) \right\} \quad (36)$$

This provides one linear relationship between the coefficients C . A second linearly independent relationship can be found by considering the slot as a transmission line, supporting transverse electromagnetic (TEM) waves. Once again, this is a good assumption providing the gap g is small compared to a wavelength. In this case, we can approximate the field E_x in the aperture to be zero, since it becomes a longitudinal component of field as far as the slot/transmission line is concerned. Combined with the boundary condition of zero tangential field E_x everywhere else on the plane $z = 0$ (due to the presence of the metal box), we can require the field E_x to equal zero everywhere in the plane $z = 0$. This is only possible in Equation 27 if we set each coefficient of $\cos \left(\frac{m\pi x}{a} \right) \sin \left(\frac{n\pi y}{b} \right)$ equal to zero. Thus we obtain, for $m = 0$,

$$\sum_{n=1}^{\infty} C_{f0n}^{TE} \left(\frac{n\pi}{b} \right) \sin \left(\frac{n\pi y}{b} \right) = 0 \quad (37)$$

Requiring

$$C_{f0n}^{TE} = 0 \quad \text{for } n = 1, 2, 3, \dots \quad (38)$$

(This is also an intuitive result for a slot illuminated by a field E_y^{inc}). For $m = 1, 2, 3, \dots$ and $n = 1, 2, 3, \dots$ we must also have

$$-C_{fmn}^{TE}\left(\frac{n\pi}{b}\right) + C_{fmn}^{TM}\left(\frac{m\pi}{a}\right) = 0 \quad (39)$$

Equations 39 and 36 are two linearly independent relationships which allow each of C_{fmn}^{TE} and C_{fmn}^{TM} to be expressed in terms of C_{fm0}^{TE} i.e.

$$\begin{bmatrix} C_{fmn}^{TE} \\ C_{fmn}^{TM} \end{bmatrix} = \begin{bmatrix} \frac{m\pi}{a} & \frac{n\pi}{b} \\ -\frac{n\pi}{b} & \frac{m\pi}{a} \end{bmatrix}^{-1} \begin{bmatrix} 2\frac{N_n}{N_0}\left(\frac{m\pi}{a}\right)C_{fm0}^{TE} \\ 0 \end{bmatrix} \quad (40)$$

Finally, given the actual aperture field $E_y^{ap_actual}(x)$, the coefficients C_{fm0}^{TE} may be found from Equation 34, by multiplying by $\sin\left(\frac{u\pi x}{a}\right)$ and integrating with respect to x from $x = 0$ to $x = a$. The result is (on replacing the dummy integer u by m),

$$\frac{b}{N_0}C_{fm0}^{TE}\left(\frac{m\pi}{a}\right)\frac{a}{2} = \int_{x_l}^{x_h} E_y^{ap_actual}(x) \sin\left(\frac{m\pi x}{a}\right) dx \quad (41)$$

Equations 41 and 40 allow all coefficients C_{fmn}^{TE} , C_{fmn}^{TM} to be deduced. These may then be inserted into Equations 26 and 27 to yield the entire field structure for E_y and E_x inside the waveguide of Figure 1, in the presence of an absorbing wall at $z = d$. It remains to find a method for estimating the field $E_y^{ap_actual}(x)$ in the aperture.

4.2 Equivalent circuit representation and the principle of reciprocity

It is tempting at this point to set the unknown aperture field $E_y^{ap_actual}(x)$ in Equation 41 to the previously calculated $E_y^{aperture}(x)$ of Equations 24 and 25. However, this will not yield correct results since the field $E_y^{aperture}(x)$ is calculated on the basis that the front panel in Figure 1 is in free space. In the presence of an enclosure in the region $z > 0$ in Figure 1 (even an infinitely long enclosure), some energy will enter the enclosure and be reflected out again via the aperture, thus altering the field $E_y^{aperture}(x)$ from its free space value. This is true even for an infinitely long waveguide, since many modes will be evanescent (particularly at low frequencies), eventually reflecting their energy back towards the aperture.

We can however use the field $E_y^{aperture}(x)$ of Equations 24 and 25 as a starting point to estimate the excitation of the different modes by a plane wave incident on the box from free space. We can then use the principle of reciprocity to estimate the reaction of the modes back on to free space, and at the same time get some measure of the extent of mode coupling that would take place if a particular mode i were incident on the aperture from within the box, resulting in a multitude of modes being reflected back into the box. The procedure is implemented by an equivalent circuit where each waveguide mode is represented by an analogous transmission line with a characteristic impedance equal to the impedance of the transverse ratio of E and H fields for the mode. The connection between the mode amplitude and the amplitude of the voltage/current waves on the analogous transmission line is made quantitative by insisting that the power flow down the analogous transmission line is equal to the power flow down the waveguide.

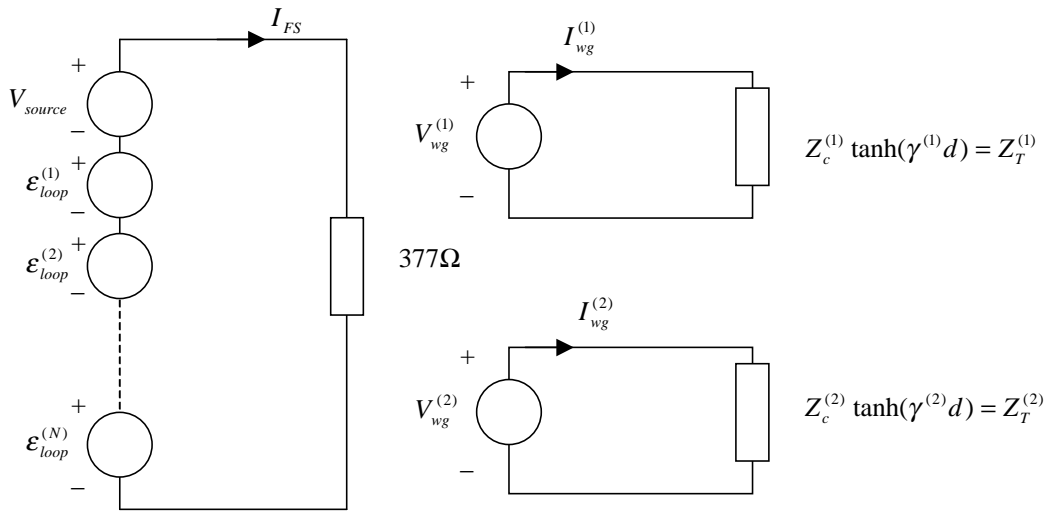


Figure 4. Equivalent circuit for experimental set up in Figure 1.

Figure 4 shows the equivalent circuit model representing the physical problem of Figure 1. For simplicity, only two waveguide modes are shown. The incident electric field in Figure 1 is represented by V_{source} , which is responsible for the main part of the current I_{FS} flowing through the 377Ω resistor (representing the impedance Z_{FS} of free space). Each of the voltage sources $V_{wg}^{(n)}$ at the start of the analogous transmission lines is made to depend on the current I_{FS} , such that in the absence of any reaction from the box (i.e. for an infinitely long transmission line), only forward travelling waves are induced on the analogous transmission lines. The precise amplitudes of these voltage waves are derived in Section 4.3. The dependence of $V_{wg}^{(n)}$ on I_{FS} is

via a transimpedance $Z_{Trans}^{(n)}$ such that $V_{wg}^{(n)} = Z_{Trans}^{(n)} I_{FS}$. The value of this transimpedance is also derived in Section 4.3. This type of coupling can also be described in terms of a mutual inductance M such that $j\omega M = Z_{Trans}^{(n)}$, and is the magnetic analogue of electric field coupling in terms of a mutual capacitance C [14]. The problem is formulated in terms of controlled voltage sources (as opposed to controlled current sources) because in the absence of any mode coupling, the slot or aperture appears as a short circuit to any modes or voltage waves incident on the slot from within the waveguide. This is a reasonable approximation to make if the slot is narrow. If controlled current sources were used, the slot would appear as an open circuit, which is not what the physical problem looks like (except possibly for very large apertures).

The principle of reciprocity can be taken into account by including reactive e.m.f.s $\mathcal{E}_{loop}^{(n)}$ in the ‘free space’ circuit, where each e.m.f. represents the reaction of a particular mode into free space. Thus if $V_{wg}^{(1)} = Z_{Trans}^{(1)} I_{FS}$, we can take the principle of reciprocity into account by setting $\mathcal{E}_{loop}^{(1)} = Z_{Trans}^{(1)} I_{wg}^{(1)}$, where $I_{wg}^{(1)}$ is the current through $V_{wg}^{(1)}$. Note that this mechanism guarantees that mode coupling will take place in the aperture: An incident mode i from within the cavity will excite $\mathcal{E}_{loop}^{(i)}$, causing current to flow through the 377Ω resistor and exciting all other forward travelling modes (including mode i itself).

The following sections outline the derivation of the expressions for $Z_{Trans}^{(n)}$ (TE and TM modes) and V_{source} , and describe how the fields internal to the box may be derived from knowledge of the terminal voltages $V_{wg}^{(n)}$.

4.3 Derivation of $Z_{Trans}^{(n)}$ and V_{source}

4.3.1 TE modes

From Equation 26, the contribution of the forward travelling TE_{mn} mode to the electric field E_y in the plane $z = 0$ of Figure 1 is given by

$$E_y|_{z=0} = C_{fmn}^{TE} \left(\frac{m\pi}{a} \right) \sin\left(\frac{m\pi x}{a} \right) \cos\left(\frac{n\pi y}{b} \right) \quad (42)$$

By equating the power transferred by the TE_{mn} mode with the power transferred down its analogous transmission line, the individual forward and reverse fields can be related to the individual forward (V_f^0) and reverse (V_r^0) voltages on the analogous transmission line by

$$E_y^{for} = -\frac{V_f^0}{Z_{mn}^{TE}} \frac{j\omega\mu_0}{\gamma_{mn}} s f_x \exp(-\gamma_{mn} z) \quad (43)$$

$$E_y^{rev} = -\frac{V_r^0}{Z_{mn}^{TE}} \frac{j\omega\mu_0}{\gamma_{mn}} s f_x \exp(+\gamma_{mn} z) \quad (44)$$

where [14]

$$f_x = \frac{\gamma_{mn}}{\left[\left(\frac{m\pi}{a} \right)^2 + \left(\frac{n\pi}{b} \right)^2 \right]} \left(\frac{m\pi}{a} \right) \sin\left(\frac{m\pi x}{a} \right) \cos\left(\frac{n\pi y}{b} \right) \quad (45)$$

$$s = \left(\frac{Z_{mn}^{TE}}{2\alpha_{mn}} \right)^{\frac{1}{2}} \quad (46)$$

$$\alpha_{mn} = \frac{-j\omega\mu_0\gamma_{mn}}{\left[\left(\frac{m\pi}{a} \right)^2 + \left(\frac{n\pi}{b} \right)^2 \right]^2} \frac{ab}{8} \left[\left(\frac{m\pi}{a} \right)^2 (1-\delta_{m0})(1+\delta_{n0}) + \left(\frac{n\pi}{b} \right)^2 (1+\delta_{m0})(1-\delta_{n0}) \right] \quad (55)$$

Equating (42) and (43) in the plane $z = 0$ results in

$$V_f^0 = -C_{fmn}^{TE} \frac{Z_{mn}^{TE}}{j\omega\mu_0 s} \left[\left(\frac{m\pi}{a} \right)^2 + \left(\frac{n\pi}{b} \right)^2 \right] \quad (48)$$

Here Z_{mn}^{TE} is the characteristic impedance $Z_c^{(n)}$ (see Figure 4) of the analogous transmission line and is given by

$$Z_{mn}^{TE} = \frac{j\omega\mu_0}{\gamma_{mn}} \quad (49)$$

We first separate out the forward and reverse waves by assuming that the plane $z = d$ in Figure 1 is perfectly absorbing, or alternatively that the waveguide dimension d is infinite. This results in forward travelling waves only, and for the case of an infinitely long waveguide effectively means that we have terminated each of the analogous transmission lines in its characteristic impedance $Z_c^{(n)}$. Later we shall reintroduce the short circuit in the plane $z = d$ and let the circuit we have derived deal naturally with any reflections that occur from the back wall. The advantage of this approach is that the rectangular cavity can then indeed be treated as a superposition of analogous transmission lines, allowing existing ILCM techniques to model the presence of a monopole or loop inside the cavity (e.g. [13][14]).

For the experimental set up in Figure 1, $\beta_x = \beta_y = 0$. From Equations 4-7, 23-25, 32, 40 and 41 it is evident that C_{fmn}^{TE} and C_{fmn}^{TM} can ultimately be related to the incident field E_y^{inc} , if we make

the initial assumption that $E_y^{ap-actual}(x) = E_y^{aperture}(x)$, in the absence of any box in the region $z > 0$ in Figure 1. We note here that for an incident plane wave travelling in a given direction $\hat{\mathbf{b}}$ with a given polarization, the field H_z^{inc} in Equation 6 is directly proportional to E_y^{inc} with a known constant of proportionality. We can therefore write

$$C_{fmm}^{TE} = k_1 E_y^{inc} \quad (50)$$

$$C_{fmm}^{TM} = k_2 E_y^{inc} \quad (51)$$

where k_1 and k_2 are known constants.

Combining Equations 48 and 50, we obtain

$$V_f^0 = -\frac{Z_{mn}^{TE}}{j\omega\mu_0 s} \left[\left(\frac{m\pi}{a} \right)^2 + \left(\frac{n\pi}{b} \right)^2 \right] k_1 E_y^{inc} \quad (52)$$

It remains to relate E_y^{inc} to I_{FS} , in the absence of any reaction from the analogous transmission lines into free space (i.e. we set all the e.m.f.s $\mathcal{E}_{loop}^{(n)} = 0$ in Figure 4). In this case, the peak power in the incident wave that impinges on the box for a $\hat{\mathbf{y}}$ polarised wave travelling in the $\hat{\mathbf{z}}$ direction is given by

$$P = \frac{(E_y^{inc})^2}{Z_{FS}} \times (ab) = I_{FS}^2 Z_{FS} \quad (53)$$

or

$$I_{FS} = \frac{E_y^{inc}}{Z_{FS}} \sqrt{ab} \quad (54)$$

Clearly this requires a source voltage (in the absence of any reactive e.m.f.s)

$$V_{source} = E_y^{inc} \times \sqrt{ab} \quad (55)$$

Finally, from Equations 54 and 52 we can write our forward travelling voltage wave in an infinitely long waveguide/analogous transmission line as

$$V_f^0 = -\frac{Z_{mn}^{TE}}{j\omega\mu_0 s} \left[\left(\frac{m\pi}{a} \right)^2 + \left(\frac{n\pi}{b} \right)^2 \right] k_1 \frac{Z_{FS}}{\sqrt{ab}} I_{FS} \quad (56)$$

V_f^0 is of course equal to one of the voltage sources $V_{wg}^{(n)}$ in Figure 4, and represents the excitation of the forward travelling TE_{mn} mode.

Equation 56 defines our transimpedance $Z_{Trans}^{(n)}$ for TE modes. It is given by

$$Z_{Trans}^{(n)} = Z_{Trans}^{TE_{mn}} = -\frac{Z_{mn}^{TE}}{j\omega\mu_0 s} \left[\left(\frac{m\pi}{a} \right)^2 + \left(\frac{n\pi}{b} \right)^2 \right] k_1 \frac{Z_{FS}}{\sqrt{ab}} \quad (57)$$

The value of V_{source} is given by Equation 55.

4.3.2 TM modes

A similar treatment for TM modes results in a transimpedance

$$Z_{Trans}^{(n)} = Z_{Trans}^{TM_{mn}} = -\frac{1}{u' \gamma_{mn}} \left[\left(\frac{m\pi}{a} \right)^2 + \left(\frac{n\pi}{b} \right)^2 \right] k_2 \frac{Z_{FS}}{\sqrt{ab}} \quad (58)$$

where

$$u' = \frac{1}{(2\alpha'_{mn} Z_{mn}^{TM})^{\frac{1}{2}}} \quad (59)$$

$$\alpha'_{mn} = \frac{-\omega\epsilon_0 j\gamma_{mn}}{\left[\left(\frac{m\pi}{a} \right)^2 + \left(\frac{n\pi}{b} \right)^2 \right] \frac{ab}{8}} \quad (60)$$

$$Z_{mn}^{TM} = \frac{\gamma_{mn}}{j\omega\epsilon_0} \quad (61)$$

γ_{mn} and k_2 are defined in Equations 28 and 51 respectively. The forward travelling voltage for a TM mode in the presence of an infinitely long waveguide is therefore given by

$$V_f^0 = Z_{Trans}^{(n)} I_{FS} \quad (62)$$

where $Z_{Trans}^{(n)}$ is given by Equation 58. V_f^0 is of course set equal to one of the voltage sources $V_{wg}^{(n)}$ in Figure 4, and represents the excitation of the forward travelling TM_{mn} mode.

5 Completion of the circuit and the reintroduction of the reflecting back wall. Reconstruction of field in cavity.

5.1 Reintroduction of reflecting back wall

Having obtained our values of $Z_{Trans}^{(n)}$ for TE modes (Equation 57) and TM modes (Equation 58), and knowing what value to assign to V_{source} for a given E_y^{inc} (Equation 55), we can complete our circuit so as to model the original problem of Figure 1. As indicated in Section 4.2, the principle of reciprocity is taken into account by including a reaction e.m.f. $\mathcal{E}_{loop}^{(n)}$ in the ‘free space’ circuit of Figure 4 for every mode excitation voltage $V_{wg}^{(n)}$, such that

$$V_{wg}^{(n)} = Z_{Trans}^{(n)} I_{FS} \quad (63)$$

$$\mathcal{E}_{loop}^{(n)} = Z_{Trans}^{(n)} I_{wg}^{(n)} \quad (64)$$

The conducting wall in the plane $z = d$ can easily be reintroduced. All that is required is to alter the ‘absorbing’ terminating characteristic impedances $Z_c^{(n)}$ for the analogous transmission lines (which have been implicitly assumed in the derivations of Section 4.1) to the impedances of the short-circuited sections of transmission line seen by the various $V_{wg}^{(n)}$. These impedances are given by $Z_T^{(n)} = Z_c^{(n)} \tanh(\gamma^{(n)} d)$, as indicated in Figure 4. The effect of this is to reflect current into the dependent voltage sources $V_{wg}^{(n)}$, causing additional excitation of the e.m.f.s $\mathcal{E}_{loop}^{(n)}$, via Equation 64. This in turn alters I_{FS} and causes $V_{wg}^{(n)}$ itself to change via Equation 63. The circuit solution of Figure 4 effectively describes what happens under steady state conditions, once all these transient effects have died down. Note that the resulting actual field $E_y^{ap-actual}(x)$ in the aperture is no longer equal to the initial field $E_y^{aperture}(x)$ of Equations 24 and 25, since the modes have been allowed to couple and therefore influence each other.

5.2 Reconstruction of the field inside the cavity

The circuit of Figure 4 may be solved for the voltages $V_{wg}^{(n)}$ using modified nodal analysis [21], noting that simple nodal analysis is inadequate because of the presence of dependent voltage sources. Alternatively, a simple algebraic manipulation of the circuit equations for Figure 4 with N modes yields the result,

$$V_{wg}^{(n)} = Z_{Trans}^{(n)} I_{FS} \quad n = 1, \dots, N \quad (65)$$

where

$$I_{FS} = \frac{-V_{source}}{\left(\sum_{n=1}^N \left\{ \frac{[Z_{Trans}^{(n)}]^2}{Z_T^{(n)}} \right\} \right) - Z_{FS}} \quad (66)$$

In the presence of a conducting wall in the plane $z = d$, it is a simple matter to decompose the terminal voltages $V_{wg}^{(n)}$ into forward (V_f^0) and reverse (V_r^0) travelling waves:

$$V_f^0 = \frac{V_{wg}^{(n)}}{1 - \exp(-2\gamma^{(n)}d)} \quad (67)$$

$$V_r^0 = \frac{V_{wg}^{(n)}}{1 - \exp(+2\gamma^{(n)}d)} \quad (68)$$

For TE modes these values of V_f^0 and V_r^0 may be used in conjunction with Equations 43 and 44 to reconstruct the total field E_y at any point inside the box due to TE modes only. For TM modes, the field E_y at any point inside the box can be found from

$$E_y^{for} = -V_f^0 u' g_y \exp(-\gamma_{mn} z) \quad (69)$$

$$E_y^{rev} = -V_r^0 u' g_y \exp(+\gamma_{mn} z) \quad (70)$$

$$g_y = \frac{\gamma_{mn}}{\left[\left(\frac{m\pi}{a} \right)^2 + \left(\frac{n\pi}{b} \right)^2 \right]} \left(\frac{n\pi}{b} \right) \sin\left(\frac{m\pi x}{a} \right) \cos\left(\frac{n\pi y}{b} \right) \quad (71)$$

(The quantity u' is defined in Equations 59-61). By summing the total fields due to forward and reverse waves for TE and TM modes, the overall total field $E_y^{Tot}(\mathbf{r})$ at any point inside the box may be calculated. The shielding effectiveness SE at that point is then given by

$$SE(\mathbf{r}) = -20 \log_{10} \left(\frac{E_y^{Tot}(\mathbf{r})}{E_y^{inc}} \right) \quad (72)$$

(N.B. Other definitions for SE may be used since we are totally ignoring E_x and E_z , though this definition will suffice for comparison with experiment and TLM).

6 Results

In this section the results of the ILCM model presented in Sections 2-5 are compared with results of numerical modelling using the transmission line matrix (TLM) method. The TLM simulations were performed using a 5mm grid. Various cases of apertures in boxes are considered, and these appear in Table 1. The aim was to consider a reasonably varied assortment of box sizes, aperture sizes and positions and field observation points, without producing an excessive amount of data. In all cases the incident field consists of a \hat{y} polarized wave travelling in the \hat{z} direction, as in Figure 1.

| Case No. | a (cm) | b (cm) | d (cm) | x_l (cm) | y_l (cm) | Slot length $x_h - x_l$ (cm) | Slot height $y_h - y_l$ (cm) | $\mathbf{r}_{obs}(x, y, z)$ (cm) | Comments on slot |
|----------|----------|----------|----------|------------|------------|---------------------------------|---------------------------------|----------------------------------|------------------|
| 1 | 48.5 | 12.0 | 48.5 | 1.5 | 10.0 | 45.5 | 1.0 | (24.25,11.75,42.25) | Near lid |
| 2 | 30.0 | 12.0 | 30.0 | 0.0 | 5.75 | 30.0 | 0.5 | (15.0,12.0,14.75) | Full width |
| 3 | 30.0 | 12.0 | 30.0 | 0.0 | 11.5 | 30.0 | 0.5 | (15.0,12.0,15.25) | Near lid |
| 4 | 30.0 | 12.0 | 30.0 | 10.0 | 6.0 | 10.0 | 0.5 | (14.75,11.75,15.25) | Central |
| 5 | 30.0 | 12.0 | 30.0 | 0.0 | 6.0 | 15.0 | 0.5 | (14.75,11.75,15.25) | Off centre |
| 6 | 20.0 | 10.0 | 30.0 | 2.0 | 1.0 | 8.0 | 1.0 | (4.75,4.75,22.25) | Off centre |
| 7 | 20.0 | 16.0 | 20.0 | 10.0 | 4.0 | 8.0 | 8.0 | (4.75,8.25,14.75) | Square |
| 8 | 20.0 | 16.0 | 20.0 | 10.0 | 4.0 | 8.0 | 1.0 | (4.75,8.25,14.75) | Off centre |
| 9 | 30.0 | 12.0 | 30.0 | 10.0 | 6.0 | 10.0 | 0.5 | (22.25,6.75,28.25) | Central (as 4) |
| 10 | 30.0 | 12.0 | 30.0 | 10.0 | 6.0 | 10.0 | 0.5 | (22.25,6.75,15.25) | Central (as 4) |

Table 1. The various cases considered for comparison of the ILCM circuit model with TLM. a , b and d are the box dimensions, while the aperture dimensions and position are determined by x_l , x_h , y_l and y_h (see Figure 1). $\mathbf{r}_{obs}(x, y, z)$ is the position inside the box where the field E_y is sampled in both the circuit model and TLM.

The circuit model and TLM values for SE as defined in Equation 72 are compared for the ten different cases in Figures 5-14. With the exception of case 7 in Figure 11, the agreement is generally seen to be excellent, both qualitatively and quantitatively. The upper frequency range considered is 3GHz, where many higher order modes are present. Simple TE₁₀ models such as [8] and [9] would be totally inadequate at such frequencies (see for example the result of the model in [8] plotted in Figure 8). In contrast, there is seen to be little deterioration in accuracy even at such high frequencies for the current model. Moreover, the model is able to cope with significantly off centre slots, something not possible with other models.

It is seen in Figure 11 (case 7) that the agreement with TLM is relatively poor (though curiously this is not true at high frequencies). This might be expected for this particular aperture since the aperture is in fact square, and cannot therefore be considered 'slot' like. The concept of the aperture forming a transmission line is likely to break down in this case, and the initial assumption of zero E_x field in the aperture (see Figure 1) is unlikely to be a good approximation.

In Figures 6-14 all modes up to $m = 5$, $n = 5$ are considered, a total of 55 modes (ignoring TE_{0n} modes where $C_{f0n}^{TE} = 0$ from Equation 38). Many of the higher order modes will be evanescent for much of the frequency range below 3GHz, and this is reflected by the fact that γ_{mn} is real. This does not however cause any difficulties with the theory, which can readily accommodate evanescent modes. The choice of $m = 5$, $n = 5$ for the upper limit on modes ensures that all propagating modes below 3GHz are included in the ILCM model in Figures 6-14. For larger boxes and/or higher frequencies it is necessary to increase the limits on m and n , and this is easily implemented in the ILCM model presented here. For example, for the large box in case 1 of Figure 5, all propagating modes below 3GHz (and a lot of extra evanescent modes) are taken into account by setting an upper limit of $m = 9$, $n = 9$. As a general rule, it is best to at least include all propagating modes up to the highest frequency of interest (in our case 3GHz), though the inclusion of some higher order evanescent modes can improve the results further (see for example [14]).

Table 2 summarises the statistics for the agreement between the circuit model and TLM in Figures 5-14. The normalised cross correlation coefficient $\rho_{dB}(0)$ is defined here as

$$\rho_{dB}(\omega_0) = \frac{\int_{-\infty}^{+\infty} S_1(\omega)S_2(\omega - \omega_0)d\omega}{\sqrt{\left\{ \int_{-\infty}^{+\infty} S_1^2(\omega)d\omega \int_{-\infty}^{+\infty} S_2^2(\omega)d\omega \right\}}} \quad (73)$$

and is always less than or equal to unity. S_1 and S_2 are the SE responses in dB. If $S_1(\omega)$ and $S_2(\omega)$ are identical then $\rho_{dB}(0) = 1$. (Indeed, $\rho_{dB}(0) = 1$ even if $S_1(\omega) = C_0 S_2(\omega)$ for some arbitrary constant C_0 , so that $\rho_{dB}(0)$ gives some measure of the similarity of the shapes of the responses $S_1(\omega)$ and $S_2(\omega)$ in dB). Excluding case 7, the overall rms difference between the curves in Figures 5-14 is 7.70dB, with a mean absolute error of 5.55dB and a correlation coefficient $\rho_{dB}(0) = 0.9440$. On an intuitive visual examination of the curves, it is clear that the agreement is very good. It is noted from Section 2.1 that the agreement in every single case in Table 2 is made worse by assuming the quasi-static impedance of [19] for the transmission line 'slot.' The overall rms difference in the latter case is 9.59dB, with a mean absolute difference of 7.08dB.

Figure 15 illustrates the level of accuracy that can reasonably be expected from the TLM technique when compared to experimental measurements. The experiment carried out here was for the scenario illustrated in case 1 of Table 1. Irradiation was via a horn antenna inside an anechoic chamber, with a monopole of length 2.5cm and diameter 1mm acting as a detector inside the box. The shielding effectiveness of the box at the location described in Table 1 was deduced from two measurements of s_{21} , with the network analyser output feeding the horn antenna and the monopole feeding the analyser input. The first (no shielding) measurement was made with only the lid of the box present to act as a ground plane for the monopole, while the second (shielded) measurement was made with the rest of the box and aperture present. A third noise floor measurement enabled an appropriate cut off point of about 500MHz to be chosen,

below which SE could not be reliably measured (i.e. the shielded measurement was below the noise floor). The rms difference between the experimental results and TLM in Figure 15 is 7.84dB, with a mean absolute error of 5.98dB and a correlation coefficient $\rho_{dB}(0) = 0.5772$. Thus the agreement with experiment exhibited by TLM is of a similar (or worse) level to the agreement of TLM with the ILCM model in Table 2. (The agreement of the ILCM model with this particular experiment is a little worse, being characterised by an rms difference of 10.10dB, mean absolute difference of 7.91dB and a correlation coefficient of just $\rho_{dB}(0) = 0.2197$). Due to the highly resonant nature of the curves and the sensitivity of the measurements to position, an rms error of 7 or 8dB is not unreasonably high: Two resonant curves which are slightly displaced will exhibit a large rms error whilst being both qualitatively and quantitatively in good agreement.

The time taken for the circuit model to reach a solution is much smaller than that taken by the numerical method of TLM. The data in each of Figures 5-14 consist of 750 frequency points separated by approximately 4MHz, with TLM taking four hours and twenty minutes to reach solution (Pentium III, 750MHz). In contrast, on the same computer the circuit model running in MATLAB (a relatively slow interpreted language) took just 30 seconds to reach solution (except for Figure 5 with the extra modes), a factor of 500 times faster. Indeed, when compiled in C++ the circuit model provides the same data in approximately 2 seconds. Combined with the 2 seconds or so required to run the subsidiary NEC simulation, this represents a speed of solution 3900 times faster than TLM.

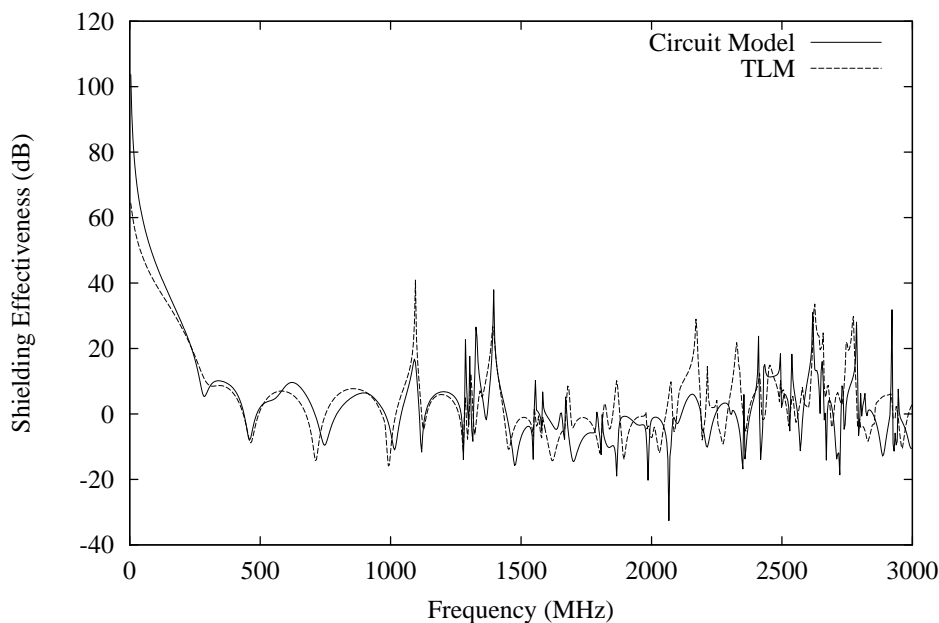


Figure 5. Comparison of the shielding effectiveness predicted by the ILCM circuit model with the numerical prediction of TLM for the box, aperture size and position indicated in Case 1 of Table 1.

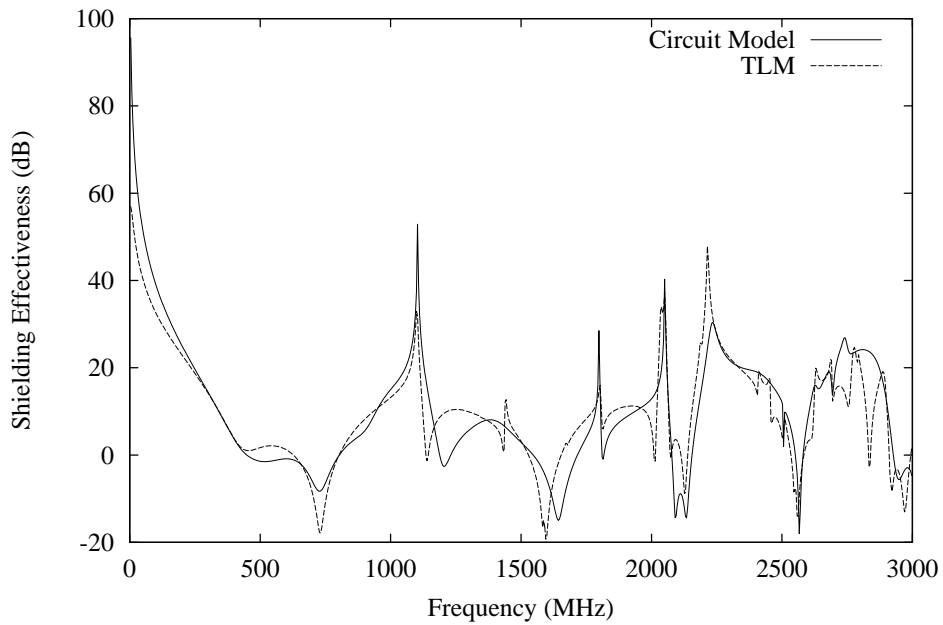


Figure 6. Comparison of the shielding effectiveness predicted by the ILCM circuit model with the numerical prediction of TLM for the box, aperture size and position indicated in Case 2 of Table 1.

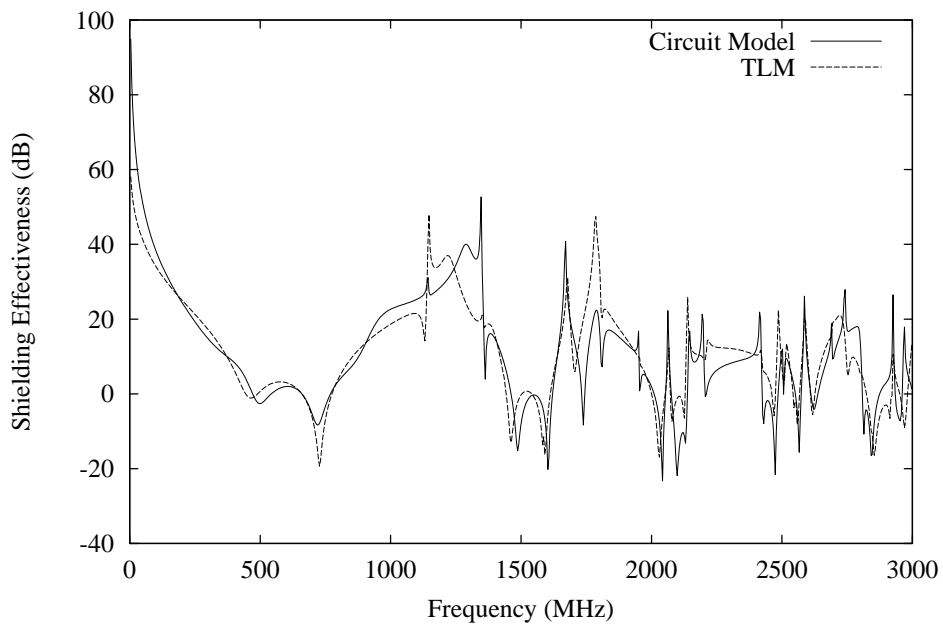


Figure 7. Comparison of the shielding effectiveness predicted by the ILCM circuit model with the numerical prediction of TLM for the box, aperture size and position indicated in Case 3 of Table 1.

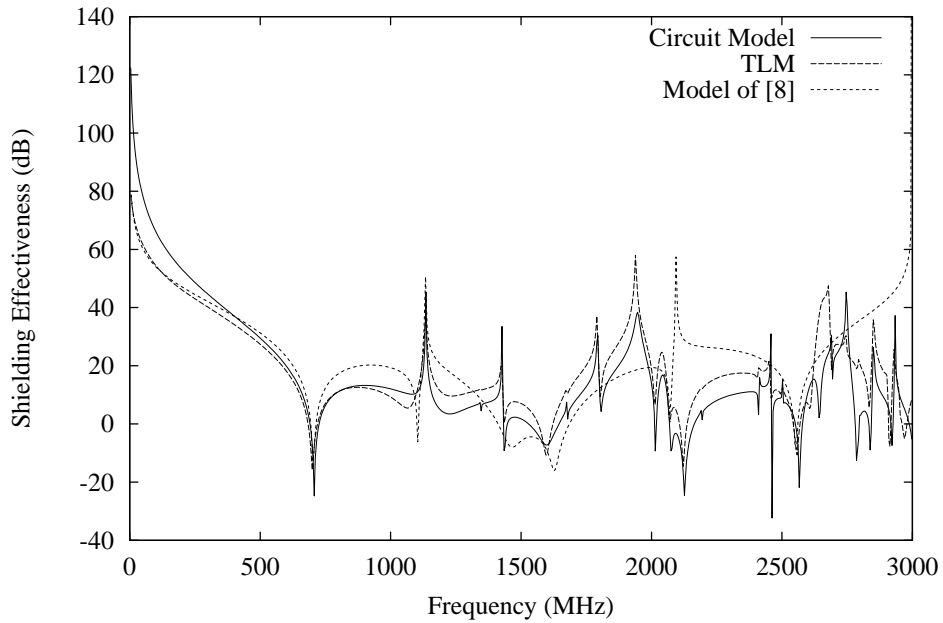


Figure 8. Comparison of the shielding effectiveness predicted by the ILCM circuit model with the numerical prediction of TLM for the box, aperture size and position indicated in Case 4 of Table 1. The prediction of the simple TE_{10} model of [8] is also shown; this is clearly seen to be inadequate at frequencies above 1GHz.

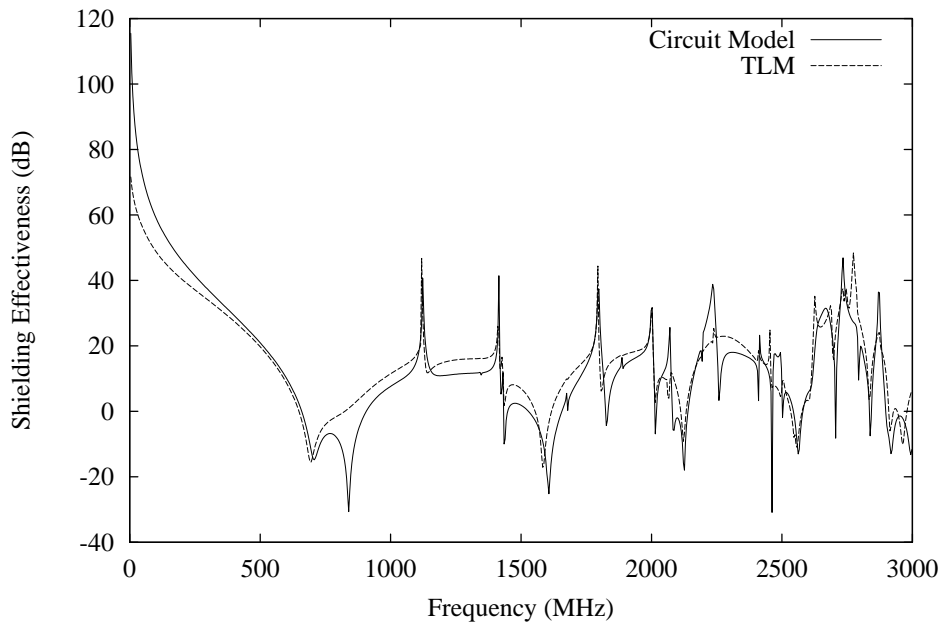


Figure 9. Comparison of the shielding effectiveness predicted by the ILCM circuit model with the numerical prediction of TLM for the box, aperture size and position indicated in Case 5 of Table 1.

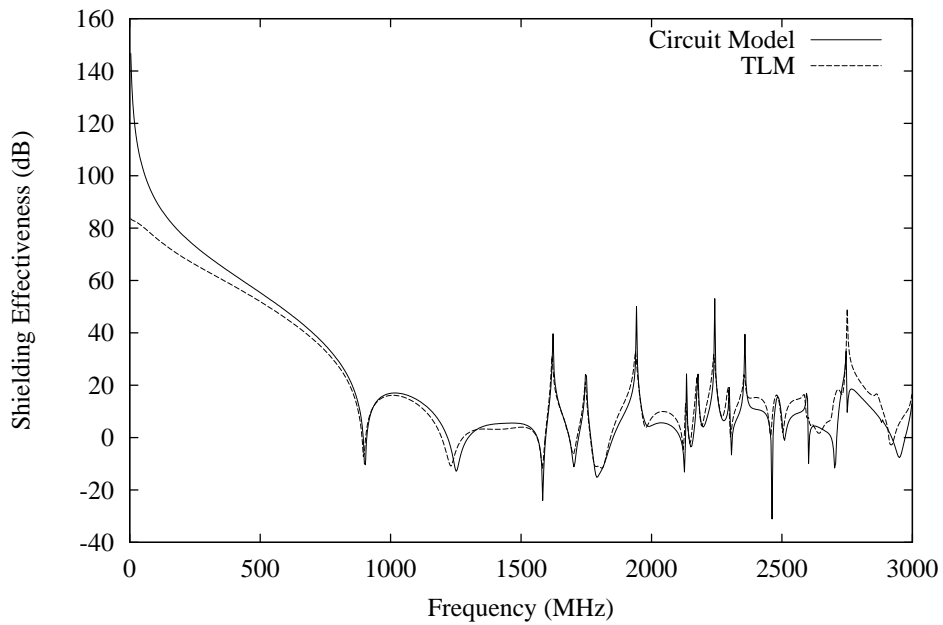


Figure 10. Comparison of the shielding effectiveness predicted by the ILCM circuit model with the numerical prediction of TLM for the box, aperture size and position indicated in Case 6 of Table 1.

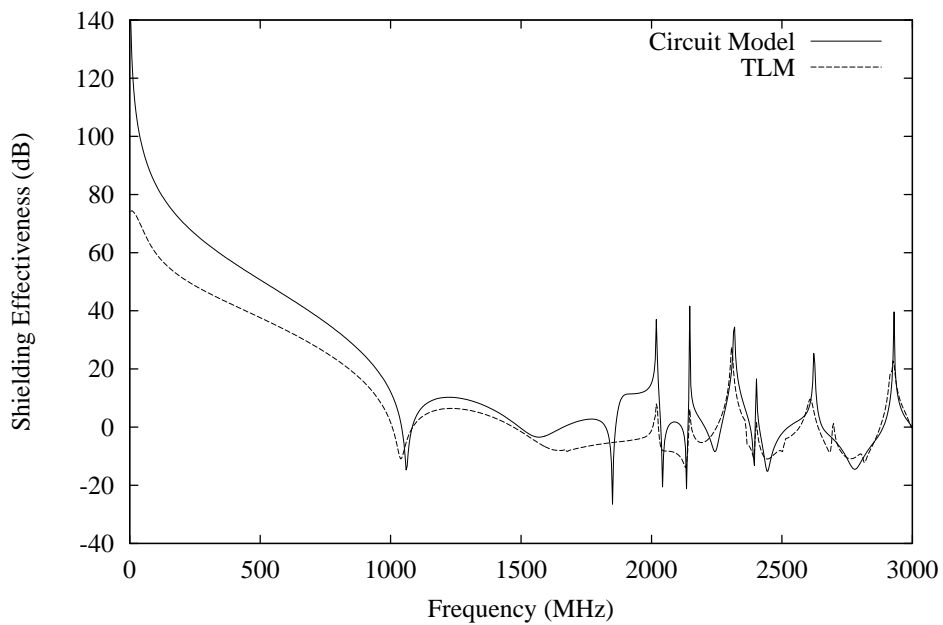


Figure 11. Comparison of the shielding effectiveness predicted by the ILCM circuit model with the numerical prediction of TLM for the box, aperture size and position indicated in Case 7 of Table 1.

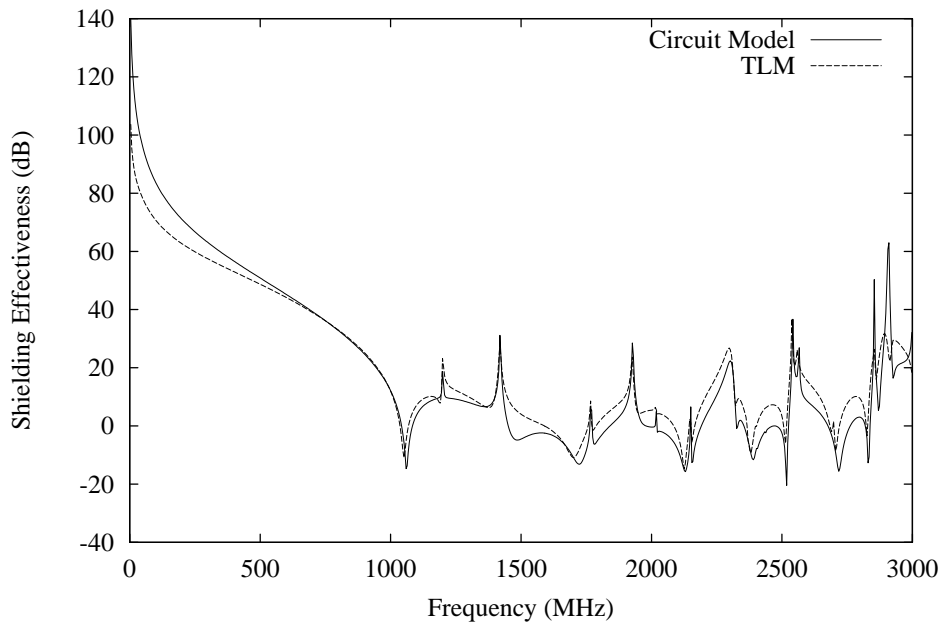


Figure 12. Comparison of the shielding effectiveness predicted by the ILCM circuit model with the numerical prediction of TLM for the box, aperture size and position indicated in Case 8 of Table 1.

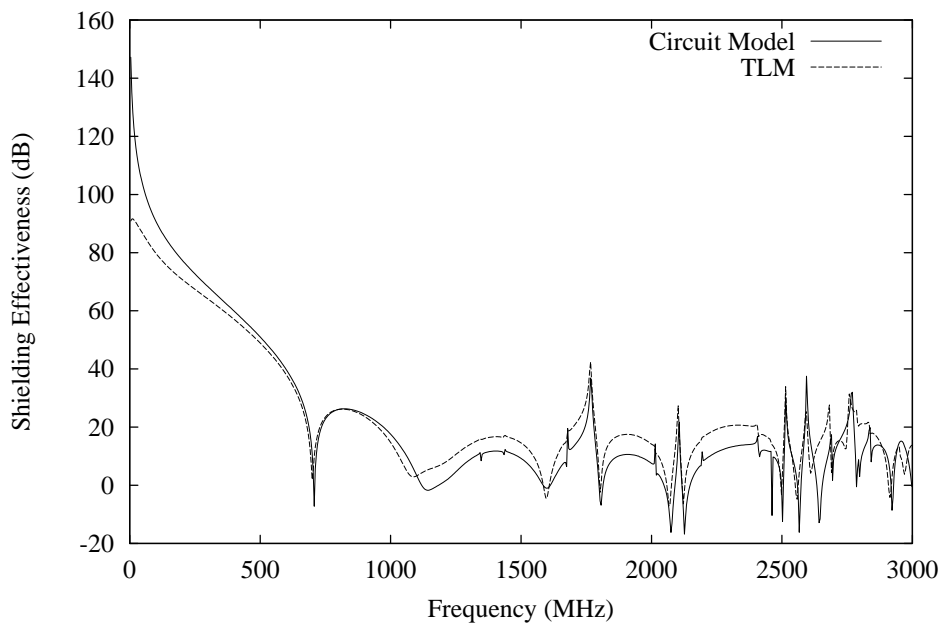


Figure 13. Comparison of the shielding effectiveness predicted by the ILCM circuit model with the numerical prediction of TLM for the box, aperture size and position indicated in Case 9 of Table 1.

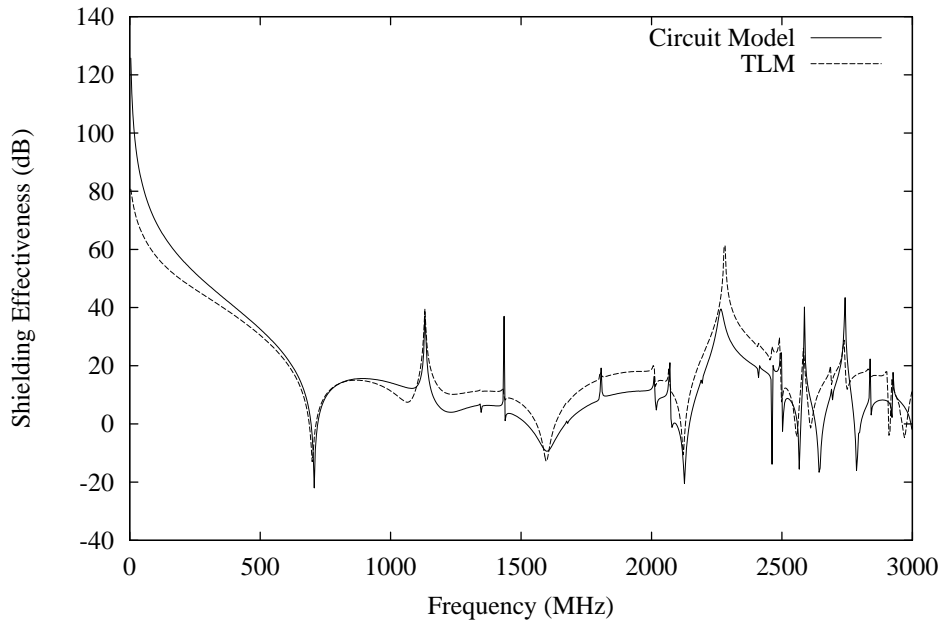


Figure 14. Comparison of the shielding effectiveness predicted by the ILCM circuit model with the numerical prediction of TLM for the box, aperture size and position indicated in Case 10 of Table 1.

| Case No. | Rms difference (dB) | Mean absolute difference (dB) | $\rho_{dB}(0)$ |
|----------------------------|---------------------|-------------------------------|----------------|
| 1 | 8.10 | 5.84 | 0.8599 |
| 2 | 6.62 | 4.59 | 0.9275 |
| 3 | 7.58 | 5.36 | 0.9161 |
| 4 | 8.49 | 6.41 | 0.9455 |
| 5 | 7.69 | 5.61 | 0.9499 |
| 6 | 7.70 | 4.85 | 0.9831 |
| 7 | 11.52 | 8.90 | 0.9763 |
| 8 | 7.08 | 5.12 | 0.9821 |
| 9 | 7.63 | 5.80 | 0.9781 |
| 10 | 8.24 | 6.38 | 0.9536 |
| Overall (Excluding case 7) | 7.70 | 5.55 | 0.9440 |

Table 2. Summary of agreement of circuit model with TLM. The table shows the rms difference, mean absolute difference and correlation coefficient for the shielding effectiveness curve predictions of the circuit model and TLM between 4MHz and 3GHz for the ten different cases considered (see Table 1 and Figures 5-14).

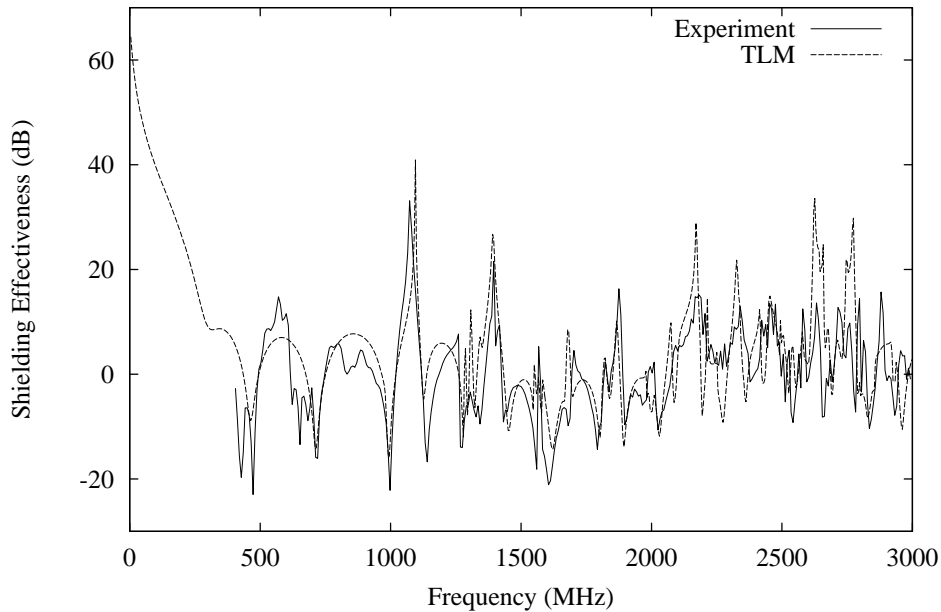


Figure 15. Comparison of the shielding effectiveness predicted by TLM with experimental results for the box, aperture size and position and observation point indicated in Case 1 of Table 1.

7 Conclusions

An intermediate level circuit model (ILCM) has been developed to model the plane wave excitation of a rectangular box containing a rectangular aperture. The model has been developed in such a way that existing ILCM techniques for modeling the presence of elements such as dipoles, monopoles, loops and transmission lines inside the box can easily be incorporated into the circuit (though for simplicity we have been concerned only with an empty box here). The ILCM model can incorporate as many higher order modes as are necessary to adequately describe the box excitation at the highest frequency of interest. Both propagating and evanescent modes are permitted. Although the model is best suited to ‘slot’ type apertures, where the slot height is a small fraction of the slot length (e.g. less than 12%), the aperture may be positioned anywhere in the front face of the box, and is not limited to the central position in height and width. The model takes into account both inter-mode coupling and reradiation into free space.

Solution times for the ILCM model are significantly less than those exhibited by traditional numerical techniques, with significantly less computer resources being required. At the same time, accuracy of the solution is not greatly affected, even at high frequencies. In our simulations, covering a variety of box and aperture sizes and positions, the ILCM model coded in MATLAB was over 500 times faster than TLM at providing a solution at 750 frequency points up to 3GHz, whilst exhibiting an rms difference of 7.70dB and mean absolute difference of 5.55dB over nine data sets. When coded in C++ the ILCM model was found to run 3900 times faster than TLM. Visual examination of the curves in Section 6 shows that the circuit model successfully predicts the vast majority of the features in the TLM simulations of shielding

effectiveness. Indeed, it is known that the latter features can be highly sensitive to position and therefore to the spatial resolution used in the TLM simulations. An rms difference of 7 or 8 dB between the ILCM model and TLM is therefore not unreasonably high. Indeed, this is the level of agreement that can be expected between a numerical TLM simulation and an experimental measurement, as illustrated in Figure 15. The main problem lies in the fact that two resonant peaks that are slightly displaced can lead to a large rms difference, when in reality there is good qualitative and quantitative agreement between the two curves, which is evident from visual inspection.

Acknowledgments

The authors wish to acknowledge that this work was made possible by support and funding from BAE Systems. Many thanks to Ian MacDiarmid.

References

- [1] R.F. Harrington and J.R. Mautz, "Characteristic modes for aperture problems," ,” *IEEE Trans. Microwave Theory Tech.*, vol. 33, no. 6, pp. 500-505, Jun. 1985.
- [2] Y. Xingchao, R.F. Harrington and J.R. Mautz, "The pseudo-image method for computing the electromagnetic field that penetrates into a cavity," *Archiv fur Elektronik und Uebertragungstechnik*, vol. 41, no. 5, pp. 307-317, Sept.-Oct. 1987.
- [3] T. Wang, R.F. Harrington and J.R. Mautz, "Electromagnetic scattering from and transmission through arbitrary apertures in conducting bodies," *IEEE Transactions on Antennas and Propagation*, vol. 38, no. 11, pp. 1805-1814, Nov. 1990.
- [4] R.F. Harrington and J.R. Mautz, "Electromagnetic coupling through apertures by the generalized admittance approach," *Computer Physics Communications*, vol. 68, pp. 19-42, Nov. 1991.
- [5] S.V. Georgakopoulos, C.R. Birtcher, and A. Balanis, "HIRF penetration through apertures: FDTD versus measurements," *IEEE Trans. Electromagn. Compat.*, vol. 43, pp. 282-294, Aug. 2001.
- [6] P. Sewell, J.D. Turner, M.P. Robinson, D.W.P. Thomas, T.M. Benson, C. Christopoulos, J.F. Dawson, M.D. Ganley, A.C. Marvin, and S.J. Porter, "Comparison of analytic, numerical and approximate models for shielding effectiveness with measurement," *IEE Proc. Sci. Meas. Technol.*, vol. 145, no.2, pp. 61-66, Mar. 1998.
- [7] W. Wallyn, D. De Zutter, and H. Rogier, "Prediction of the shielding and resonant behaviour of multisection enclosures based on magnetic current modeling," *IEEE Trans. Electromagn. Compat.*, vol. 44, pp. 130-138, Feb. 2002.

- [8] M.P. Robinson, T.M. Benson, C. Christopoulos, J.F. Dawson, M.D. Ganley, A.C. Marvin, S.J. Porter, and D.W.P. Thomas, "Analytical formulation for the shielding effectiveness of enclosures with apertures," *IEEE Trans. Electromagn. Compat.*, vol. 40, pp. 240-248, Aug. 1998.
- [9] R. Azaro, S. Caorsi, M. Donelli, and G.L. Gragnani, "Evaluation of the effects of an external incident electromagnetic wave on metallic enclosures with rectangular apertures," *Microwave Opt. Technol. Lett.*, vol. 28, no. 5, pp. 289-293, Mar. 2001.
- [10] R. Azaro, S. Caorsi, M. Donelli, and G.L. Gragnani, "A circuital approach to evaluating the electromagnetic field on rectangular apertures backed by rectangular cavities," *IEEE Trans. Microwave Theory Tech.*, vol. 50, pp. 2259-2266, Oct. 2002.
- [11] S. Ramo, J.R. Whinnery, and T. Van Duzer, *Fields and waves in communication electronics*, 3rd ed. New York: John Wiley and Sons, Inc., 1994.
- [12] I. Belokour and J. LoVetri, "A 2D-Transmission line model for the EM field estimation inside enclosures with apertures," in *Proc. IEEE Int. Symp. Electromagnetic Compatibility*, Minneapolis, MN, Aug. 2002, pp. 424-429.
- [13] I.D. Flintoft, N.L. Whyman, J.F. Dawson, and T. Konefal, "Fast and accurate intermediate level modeling approach for EMC analysis of enclosures," *IEE Proc. Sci. Meas. Technol.*, vol. 149, no.5, pp. 281-285, Sep. 2002.
- [14] T. Konefal, J.F. Dawson, A.C. Denton, T.M. Benson, C. Christopoulos, A.C. Marvin, S.J. Porter, and D.W.P. Thomas, "Electromagnetic coupling between wires inside a rectangular cavity using multiple mode analogous transmission line circuit theory," *IEEE Trans. Electromagn. Compat.*, vol. 43, pp. 273-281, Aug. 2001.
- [15] T. Konefal, J.F. Dawson, A.C. Denton, T.M. Benson, C. Christopoulos, A.C. Marvin, S.J. Porter, and D.W.P. Thomas, "Electromagnetic fields produced by PCB stripline and microstrip inside a screened rectangular enclosure: A circuit approach," in *Proc. 4th Eur. Symp. Electromagnetic Compatibility*, vol. 1, Brugge, Belgium, Sep. 2000, pp. 587-592.
- [16] D.F. Williams, L.A. Hayden, and R.B. Marks, "A complete multimode equivalent circuit theory for electrical design," *Journ. Res. Natl. Inst. Stand. Technol.*, vol. 102, no. 4, pp. 405-423, Aug. 1997.
- [17] G.J. Burke and A.J. Poggio, "Numerical electromagnetics code (NEC) – Method of moments," Tech. Doc. 116, Naval Ocean Systems Centre, San Diego, CA, Jan. 1981.
- [18] J.A. Kong, *Electromagnetic wave theory*, New York: John Wiley and Sons, Inc., 1986, ch. 5.
- [19] K.C. Gupta, R. Garg, and I.J. Bahl, *Microstrip Lines and Slotlines*, Norwood, MA: Artech House, 1979, ch 7.

[20] T. Konefal, J.F. Dawson, A.C. Denton, T.M. Benson, C. Christopoulos, A.C. Marvin, S.J. Porter, and D.W.P. Thomas, "Electromagnetic field predictions inside screened enclosures containing radiators," in *Proc. IEE Conf. Electromagnetic Compatibility*, vol. 464, York, UK, Jul. 1999, pp. 95-100.

[21] W.J. McCalla, *Fundamentals of computer aided circuit simulation*, 4th ed. Norwell, MA: Kluwer Academic Publishers, 1997.